A novel polarization interferometer for measuring upper atmospheric winds*

Mu Ting-Kui(穆廷魁) and Zhang Chun-Min(张淳民)†

MOE Key Laboratory for Nonequilibrium Synthesis and Modulation of Condensed Matter, School of Science, Xi'an Jiaotong University, Xi'an 710049, *China*

(Received 2 March 2009; revised manuscript received 10 January 2010)

A static polarization interferometer for measuring upper atmospheric winds is presented, based on two Savart plates with their optical axes perpendicular to each other. The principle and characteristics of the interferometer are described. The interferometer with a wide field of view can offer a stable benchmark optical path difference over a specified spectral region of 0.55–0.63 μm because there are no quarter wave plates. Since the instrument employs a straight line common-path configuration but without moving parts and slits, it is very compact, simple, inherently robust and has high throughput. The paper is limited to a theoretical analysis.

Keywords: polarization interferometer, upper atmospheric winds, optical path difference
PACC: 0760L, 0765, 4225J, 4225L

1. Introduction

Temperatures and winds play a major role in the dynamics of the atmosphere, and their measurement still presents some challenges. The sources for measuring upper atmosphere winds are aurora and airglow whose height is 80–300 km from the ground,[1,2] so passive optical methods are highly attractive at these heights, because the sources offer natural Doppler targets from a variety of altitudes, and the instruments have the potential to be used for measuring rays from space.[3] There are two measuring spectral lines that mainly come from the excitation of atomic oxygen in metastable states: the excitation from O (^{1}S) to O (^{1}D) produces a 557.7-nm ray and the excitation from O (^{1}D) to the basic state produces a 630-nm ray; their lifetimes are about 1 s and 140 s respectively.

The optimal instruments used for measuring upper atmospheric winds should have some features such as compactness, achromaticity, robustness, stability, and high sensitivity, etc. Some instruments have been developed,[1−8] therein the Michelson interferometer offers an interesting alternative because it can be field-widened. The first wide-angle Michelson interferometer (WAMI) for the measurement of atmospheric temperature was presented by Hilliard and Shepherd;[1] the interferometer is set to a single path difference for which the field-widening conditions can readily be met. Later on, the WAMI concept was extended to the measurement of winds as well as temperatures in an instrument selected for space shuttle flight, called the wide-angle Michelson Doppler imaging interferometer (WAMDII).[2] A modified version of the WAMDII called the WINDII was launched on the Upper Atmosphere Research Satellite on 12 September 1991.[3] The MICADO presented by Thuillier and Herse[7] is also a field-widened instrument that has been used to measure upper atmospheric winds and temperatures. However, the above instruments have all been non-polarising systems.

The first polarizing interferometer described by Title and Ramsey was used as filter elements in which the tuning was used to select a particular line.[9] The polarizing atmospheric Michelson interferometer (PAMI), combining the polarization tuning technique of Title and Ramsey with Shepherd's[2] technique of deriving winds from intensity measurements at sequential path differences, is achieved by observing the output intensity as in WAMDII but changing the optical path difference (OPD) by rotating a polarizer external to the optics rather than moving a mirror. This scanning system, used in the PAMI, is much simpler than the moving mirror system of WAMDII. Another PAMI was described by Bird *et al.*[10] which lends it-

*Project supported by the National Natural Science Foundation of China (Grant No. 40875013), the National Defense Basic Scientific Research Project (Grant No. A1420080187), the National High Technology Research and Development Program of China (Grant No. 2006AA12Z152) and the State Key Program of National Natural Science Foundation of China (Grant No. 40537031).
†Corresponding author. E-mail: zcm@mail.xjtu.edu.cn
© 2010 Chinese Physical Society and IOP Publishing Ltd

self to making simultaneous measurements at different phase steps rather than sequentially; this capability would be particularly useful for time-varying sources. However, the system can be operated only at a special wavelength due to the use of quarter wave plates, and the main drawback is that the phase retardation of the quarter wave plates is highly insensitive to the incident angle and thus will introduce some errors when the system works under wide-angle conditions.

The interference method for measuring upper atmospheric winds can be found in several papers.[1,2,11−19] The main parameters given by interferometers are one benchmark OPD which is equal to the integral multiple of a wavelength, and four increment OPDs in steps of quarter wavelength from zero. To accomplish the above acquisition, we present a static polarization interferometer. The instrument without half wave plate can be operated over a wide spectral region. Compared to the Michelson interferometers, our system, which employs a straight line common-path configuration, is compact without moving parts. A further advantage is that the instrument can be operated over a wide field of view (FOV) and thus has high throughput.

2. Instrumental principle

The basic polarization interferometer concept is depicted in Fig. 1(a), where the image of an extended scene is collimated by a fore-optical system (L_0, L_1) to form a beam incident on a linear polarizer P_1 with its polarization oriented at 45° to the axis of the left Savart plate. The beam consequently is split into two polarized components with the same amplitudes by the left Savart plate and reunited by the right Savart plate. The analyser P_2, with its polarization oriented parallel with P_1, resolves the two components into a common polarization state. The beams then pass on to the phase mask and sensor portion of the setup, which are then phase shifted via the polarizing wire grids in the pixilated mask.[20] The intensities of the four fringe patterns are simultaneously recorded by a detector located at the focal plane of imaging lens L_2. Therein, how to use the pixilated mask and simultaneously record four intensities is not the content of this paper.

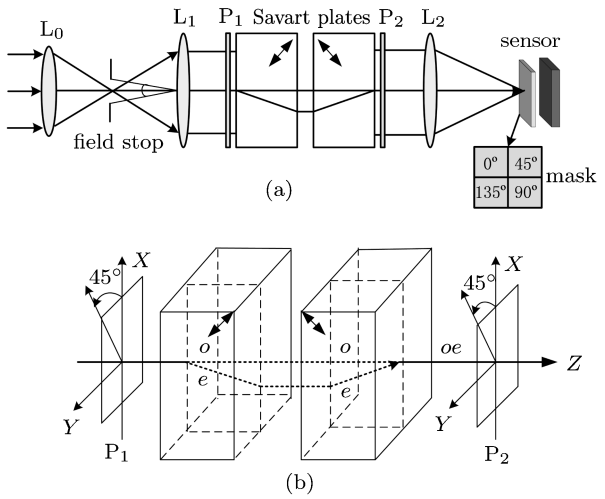


Fig. 1. (a) Conceptual diagram of the polarization interferometer and (b) coordinate system of the two Savart plates.

The key component in the interferometer is the two Savart plates. Figure 1(b) shows its coordinate system. Two identical Savart plates cut at 45° to the optical axis and have their principal sections parallel, but the two optic axes are perpendicular to each other. The *o*-ray in the left plate with its vibrations perpendicular to the principal section is still an *o*-ray in the second plate since the principal sections of the two plates are parallel. Likewise, the *e*-ray in the first plate is still an *e*-ray in the second plate. Then the OPD of the two polarized components is introduced after light passes through the Savart plates.

The OPD between two polarized components introduced by a single Savart plate is given by[21−42]

$$\Delta_1 = t \times \left(\frac{1}{C} - \frac{1}{b}\right) + t \times \frac{a^2 - b^2}{a^2 + b^2} \cos\omega \sin i + t \times \frac{\sin^2 i}{2} \left[\left(b - \frac{a^2}{C}\right) \sin^2 \omega + \left(b - \frac{a^2 b^2}{C^3}\right) \cos^2 \omega\right], \quad (1)$$

where $C = [(a^2 + b^2)/2]^{1/2}$, $a = 1/n_e$, $b = 1/n_o$; n_o and n_e are the refractive indices of the Savart plate for the *o*- and *e*-rays, respectively; t is the thickness of one Savart plate; i is the incident angle, and ω is the angle between the incident plane and the principal section of the left Savart plate. Thus, the total OPD for the two similar Savart plates is

$$\Delta = 2t \times \left(\frac{1}{C} - \frac{1}{b}\right) + 2t \times \frac{a^2 - b^2}{a^2 + b^2} \cos\omega \sin i + t \times \sin^2 i \left[\left(b - \frac{a^2}{C}\right) \sin^2 \omega + \left(b - \frac{a^2 b^2}{C^3}\right) \cos^2 \omega\right]. \quad (2)$$

Therefore, the benchmark OPD can be presented as

$$\Delta_0 = 2t \times \left(\frac{1}{C} - \frac{1}{b}\right), \tag{3}$$

then the deviation part of the benchmark OPD is

$$\begin{aligned}\delta\Delta &= \Delta - \Delta_0 \\ &= 2t \times \frac{a^2 - b^2}{a^2 + b^2} \cos\omega \sin i + t \\ &\quad \times \sin^2 i \left[\left(b - \frac{a^2}{C}\right) \sin^2 \omega \right. \\ &\quad \left. + \left(b - \frac{a^2 b^2}{C^3}\right) \cos^2 \omega \right]. \end{aligned} \tag{4}$$

According to the measurement principle,[2] we need to ensure that

$$|\delta\Delta| \leq \lambda, \tag{5}$$

and

$$\Delta_0 = m\lambda \quad m = \pm 1 \pm 2, \ldots, \tag{6}$$

then we can obtain

$$\begin{aligned}&\left|\frac{2(a^2 - b^2)}{a^2 + b^2} \cos\omega \sin i + \sin^2 i \left[\left(b - \frac{a^2}{C}\right) \sin^2 \omega \right.\right. \\ &\left.\left. + \left(b - \frac{a^2 b^2}{C^3}\right) \cos^2 \omega \right]\right| \leq \left|\frac{2}{m}\left(\frac{1}{C} - \frac{1}{b}\right)\right|. \end{aligned} \tag{7}$$

Therefore, equations (5)–(7) are the qualification of the benchmark OPD.

3. Characteristics of the interferometer

3.1. Optimal material

If we assume that the benchmark OPD at a wavelength of 630 nm is $\Delta_0 = 2.2$ mm, and the Savart plate is made of calcite crystal with the ordinary index $n_o = 1.656$ and the extraordinary index $n_e = 1.486$, we can find that the thickness of a single Savart plate is $t \approx 12$ mm, and $m \approx 3.5 \times 10^3$. According to Eq. (1), the OPD Δ as a function of angles i and ω can be shown in Fig. 2(a). It is found that the OPD varies largely with the incident angle when $\omega = 0$ or π, but the variation is very small when $\omega = \pi/2$. Figure 2(b) shows the deviation part of OPD, $\delta\Delta$, as a function of the incident angle. As can be seen, $\delta\Delta$ is less than 0.63 μm over the half FOV of 1.3 degrees. Since the available half FOV of the calcite interferometer is very small, the corresponding throughput is not high.

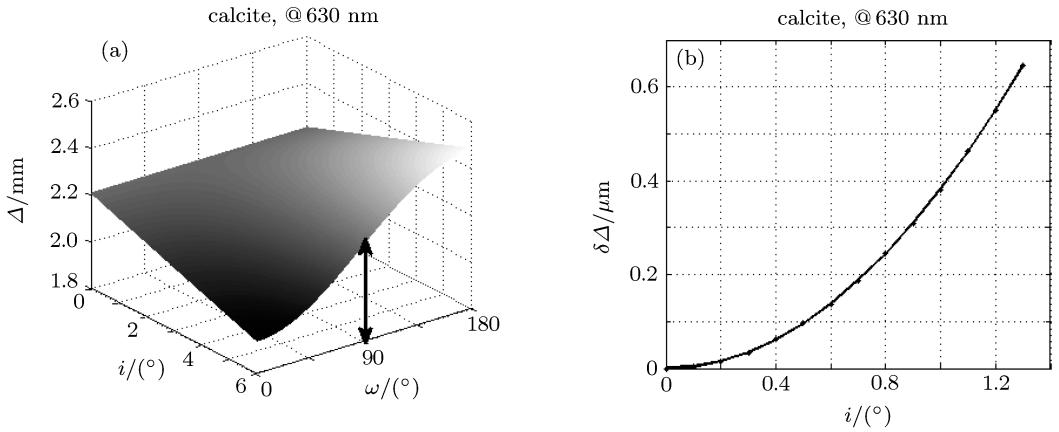


Fig. 2. (a) The total OPD Δ as a function of incident angle i and the angle between the incident plane and the principal section of the left Savart plate ω; (b) the deviation part of OPD, $\delta\Delta$ as a function of i when $\omega = \pi/2$ (calcite, @630.0 nm).

If we assume that the benchmark OPD at a wavelength of 557.7 nm is $\Delta_0 = 107.5$ μm, and the Savart plate is made of quartz crystal with the ordinary index $n_o = 1.543$ and the extraordinary index $n_e = 1.552$, we can obtain the thickness of a single Savart plate $t \approx 12$ mm, and $m \approx 193$. Figure 3(a) shows the OPD, Δ, as a function of the angles i and ω. The OPD varies very little with the incident angle i when $\omega = \pi/2$. Figure 3(b) shows the deviation part of the OPD, $\delta\Delta$, as a function of the incident angle i when $\omega = \pi/2$; the maximum OPD is less than 0.5577 μm over the half FOV of 5.2 degrees. Compared with the calcite interferometer, the available half FOV of the quartz interferometer is very large and thus the corresponding throughput is also high.

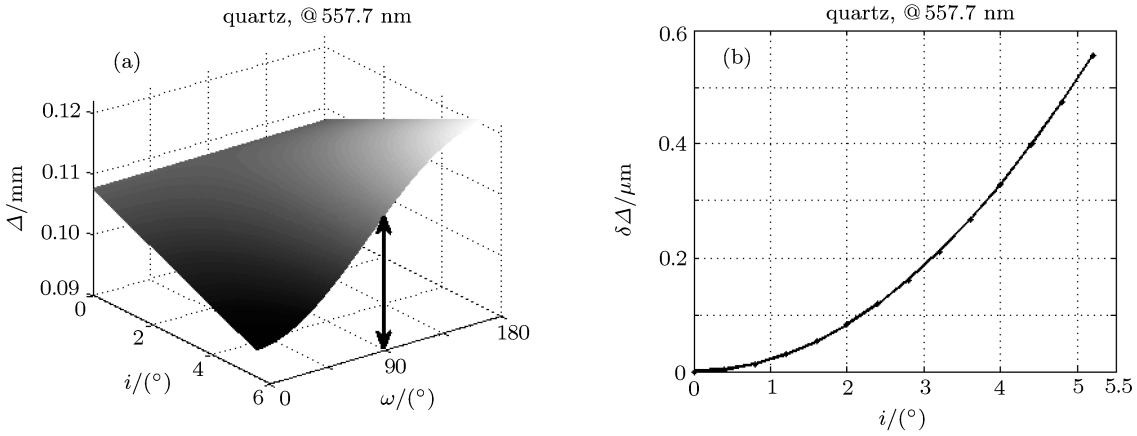


Fig. 3. (a) The total OPD Δ as a function of incident angle i and the angle between the incident plane and the principal section of the left Savart plate ω; (b) the deviation part of the OPD, $\delta\Delta$, as a function of i when $\omega = \pi/2$ (quartz, @557.7 nm)

As discussed above, to widen the FOV of the interferometer, we should choose some special material with a small birefringence index, such as quartz, sapphire, MgF_2, ADP, KDP, etc.

3.2. FOV and visibility

It is clear that for a perfectly monochromatic source and a pinhole aperture, $V = 1$, but as the aperture is made finite, the superposition of fringes of varying $\delta\Delta$ causes the visibility to decrease to a value that we shall call the FOV visibility parameter, denoted by V_{FOV}. The FOV may be divided into annular segments, each of which has an OPD different from that of its immediate neighbours by a small amount. The contribution to the fringe pattern from a single segment can be represented by a vector with an amplitude proportional to the area of the segment, and a phase angle $2\pi\delta\Delta/\lambda$ corresponding to the value of $(\Delta - \Delta_0)$ for that segment.

Because the two polarized components split by the Savart plates have the same amplitudes, and have the same vibration direction after they pass through analyser P_2, the distribution of intensity resulting from the superposition of the two polarized components is

$$I = 2I_0[1 + \cos(2\pi\sigma\Delta)]. \tag{8}$$

Substituting Eq. (2) into Eq. (8), we can have the distribution of the fringe patterns as shown in Fig. 4. As can be seen, for the calcite interferometer the visibility is very good over the half FOV of 5 degrees, while for the quartz interferometer the visibility is very good over the half FOV of 22 degrees.

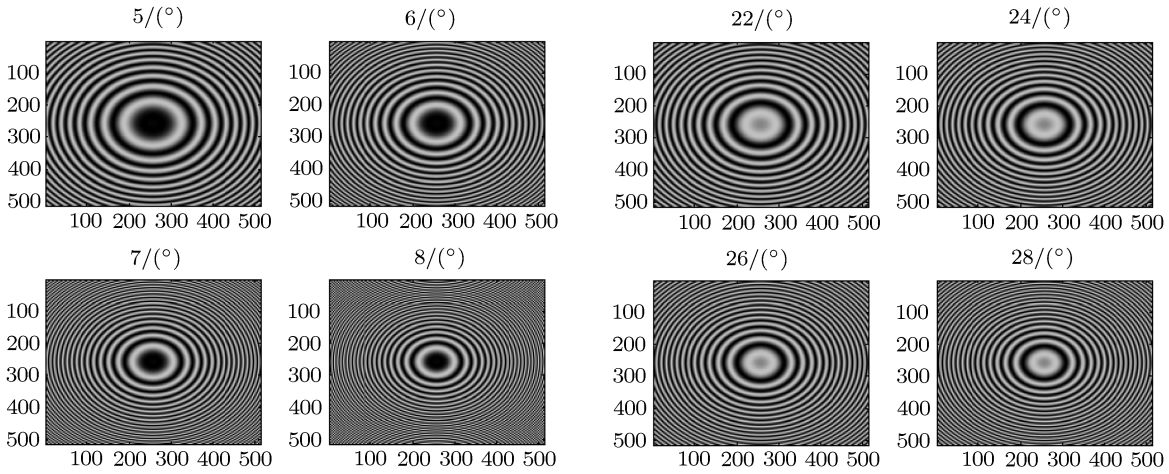


Fig. 4. Distribution of fringe patterns in different FOV when $\omega = \pi/2$. (a) In the calcite interferometer @630 nm and (b) in the quartz interferometer @557.7 nm.

3.3. Throughput

For monochromatic radiation the radiant flux I_0 carried by an extended source is[43]

$$I_0 = T(\lambda)B(\lambda)A\Omega, \tag{9}$$

where $T(\lambda)$ is the transmission of the optical system; $B(\lambda)$, the radiance of the source; Ω, the solid angle subtended by the source; and A, the area of the interferometer's aperture. According to the definition of the throughput,[44] we have

$$E = A\Omega. \tag{10}$$

In our system there is no narrow slit, the slit is replaced by the field view stop, thus, the throughput is limited only by the detector at the focal plane of the Fourier lens L_2, and the solid angle subtended by L_2 is given by

$$\Omega = \pi r_2^2/f_2^2, \tag{11}$$

where r_2 and f_2 are the radius and focal length of the lens L_2, respectively. Then the throughput E can be given by

$$E_{\rm p} = \pi w_{\rm d} l_{\rm d} r_2^2/f_2^2, \tag{12}$$

where $w_{\rm d}$ and $l_{\rm d}$ are the width and length of the detector, respectively.

For comparison, we use the same parameters for the fore-optical collimator L_2 in a Sagnac interferometer with an entrance slit.[45] Because the slit is in the back focal plane of L_2, the throughput is limited by the area of the slit; the solid angle subtended by the slit from the lens L_2 is

$$\Omega = w_{\rm s} l_{\rm s}/f_2^2, \tag{13}$$

where $w_{\rm s}$ and $l_{\rm s}$ are the width and length of the slit, respectively. Thus the throughput is given by

$$E_{\rm s} = \pi w_{\rm s} l_{\rm s} r_2^2/f_2^2. \tag{14}$$

From Eqs. (12) and (14) we can obtain

$$E_{\rm p}/E_{\rm s} = (w_{\rm d} l_{\rm d})/(w_{\rm s} l_{\rm s}). \tag{15}$$

Assume that the Sagnac interferometer and our system have the same spatial resolution for the direction perpendicular to the slit and cross-track; and $w_{\rm d} = N w_{\rm s}$, where N is the column number of the charge coupled device. Because in the Sagnac interferometer the slit is on the back focal plane of the fore-optical lens L_2, and in our system the detector is on the back focal plane of L_2, we have $l_{\rm s} = l_{\rm d}$, and then

$$E_{\rm p}/E_{\rm s} = N. \tag{16}$$

That is, N times more power can be attained by our system than the Sagnac interferometer with a slit.

The intensity of the light becomes $I_0/2$ after passing through an ideal polarizer P_1; if the two Savart plates are ideal, there will be no energy loss when light passes through them, but the light is divided into two beams, and the intensity of each beam becomes $I_0/4$. After passing through the analyser P_2, the intensity of each beam becomes $I_0/8$. We can use a quarter-wave-plate with their fast axes oriented at 45° to displace P_2 then transform the linearly polarized light into right- and left-hand circularly polarized light beams. This circularly polarized light is then phase shifted via the polarizing wire grids in the pixilated mask.

3.4. Dispersion effects

Since the detection wavelengths of our system are 557.7 nm and 630 nm, and the Savart plates are made of uniaxial crystal, the refractive indices of the *e*- and *o*-rays must vary with wavelength. According to Eq. (1), the dispersion will have some influence on the OPD.

Unless specified, the refractive indices are the average values for standard daylight or the values measured at 632.8 nm at room temperature (the difference between the daylight and He–Ne values are within 0.1%). Assuming that the Savart plates are made of quartz, refractive indices at specific wavelengths within specified ranges can be derived from dispersion formulae given in the *Handbook of Optics*,[46]

$$\begin{aligned} n_o^2 = 1 &+ \frac{0.663044\lambda^2}{\lambda^2-(0.06)^2} + \frac{0.517852\lambda^2}{\lambda^2-(0.106)^2} \\ &+ \frac{0.175912\lambda^2}{\lambda^2-(0.119)^2} + \frac{0.56538\lambda^2}{\lambda^2-(8.844)^2} \\ &+ \frac{1.675299\lambda^2}{\lambda^2-(20.742)^2}, \end{aligned} \tag{17}$$

and

$$\begin{aligned} n_e^2 = 1 &+ \frac{0.665721\lambda^2}{\lambda^2-(0.06)^2} + \frac{0.503511\lambda^2}{\lambda^2-(0.106)^2} \\ &+ \frac{0.214792\lambda^2}{\lambda^2-(0.119)^2} + \frac{0.539173\lambda^2}{\lambda^2-(8.792)^2} \\ &+ \frac{1.807613\lambda^2}{\lambda^2-(197.7)^2}, \end{aligned} \tag{18}$$

where λ is the wavelength in μm. Assuming that the thickness of the Savart plate is $t \approx 12$ nm, the angle between the incident plane and the principal section of the left Savart plate is $\omega = \pi/2$, and the incident angle $i = 5.5°$. Substituting Eqs. (17) and (18) into Eq. (2), we can obtain the relationship between the total OPD, Δ, and the wavelength as shown in Fig. 5. As can be seen, the OPD, Δ, increases with wavelength, and the maximum difference is $\Delta(0.63\ \mu\text{m}) - \Delta(0.55\ \mu\text{m}) = 0.3\ \mu$m, which is less than λ. So the system is achromatic over the spectral region of 0.55–0.63 μm.

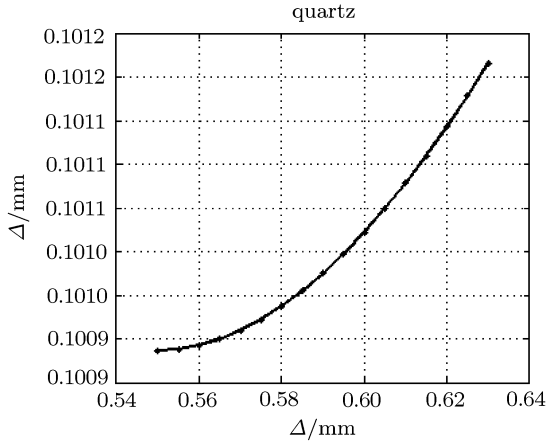


Fig. 5. The relationship between the total OPD Δ and the wavelength when $\omega = \pi$ / 2 (quartz).

4. Conclusions

In this paper, we present a static polarization interferometer based on two Savart plates. The system could theoretically be made very small with all the following advantages: stable benchmark OPD, large field of view, high optical throughput, achromatic, but without the usual problems: sensitivity to vibration, limit to a special wavelength, requirement for precise and expensive scanning mechanism; and these characteristics will enable the deployment of this type of system in new situations. Careful material choice for the Savart plates will allow the construction of the system to widen the FOV. However, the study in the paper is only limited to the theoretical analysis, and the experimentation and practical considerations will be addressed in a future manuscript.

References

[1] Hilliard R L and Shepherd G G 1966 *J. Opt. Soc. Am.* **56** 362

[2] Shepherd G G, Gault W A, Miller D W, Pasturczyk Z, Johnston S F, Kosteniuk P R, Haslett J W, Kendall D J W and Wimperis J R 1985 *Appl. Opt.* **24** 1571

[3] Shepherd G G, Thuillier G, Gault W A, Solheim B H, Hersom C, Alunni J M, Brun J F, Charlot P, Cogger L L, Desaulniers D L, Evans W F J, Gattinger R L, Girod F, Harvie D, Hum R H, Kendall D J W, Llewellyn E J, Lowe R P, Ohrt J, Pasternak F, Peillet O, Powell I, Rochon Y, Ward W E, Weins R H and Wimperis J 1993 *J. Geophys. Res.* **98** 10725

[4] Hernandez G and Roble R G 1979 *Appl. Opt.* **18** 3376

[5] Hays P B, Killeen T L, Spencer N W, Wharton L E, Roble R G, Emery B A, Fuller-Rowell T J, Rees D, Frank L A and Craven J D 1984 *J. Geophys. Res.* **89** 5597

[6] Killeen T L and Roble R G 1988 *Rev. Geophys.* **26** 329

[7] Thuillier G and Herse M 1988 *Appl. Opt.* **30** 1210

[8] Hays P B, Abreu V J, Dobbs M E, Gell D A, Grassl H J and Skinner W R 1993 *J. Geophys. Res.* **98** 10713

[9] Title A M and Ramsey H E 1980 *Appl. Opt.* **19** 2046

[10] Birdt J C, Liangt F, Solheim B H and Shepherd G G 1995 *Meas. Sci. Technol.* **6** 1368

[11] He J and Zhang C M 2005 *J. Opt.* A: *Pure Appl. Opt.* **7** 613

[12] Zhang C M and He J 2006 *Opt. Express* **14** 12561

[13] Zhang C M, Zhao B C, Xiang L B and Li Y C 2006 *Optik* **117** 265

[14] Zhang C M, Zhao B C, Li Y C and Ye J Y 2007 *SPIE* **6279** 62791D

[15] Tang Y H, Zhang C M, Liu H C, Chen G D and He J 2005 *Acta Phys. Sin.* **54** 4065 (in Chinese)

[16] Ye J Y, Zhang C M, Zhao B C and Li Y C 2008 *Acta Phys. Sin.* **57** 67 (in Chinese)

[17] Ruan K, Zhang C M and Zhao B C 2008 *Acta Phys. Sin.* **57** 5435 (in Chinese)

[18] Bu Z C, Zhang C M, Zhao B C and Zhu H C 2009 *Acta Phys. Sin.* **58** 2415 (in Chinese)

[19] Bu Z C, Zhang C M and Zhao B C 2009 *SPIE* **7156** 71563D

[20] Matt N, Millerd J, Brock N, North-Morris M, Hayes J and Wyant J 2005 *Appl. Opt.* **44** 6861

[21] Françon M and Mallick S 1971 *Polarisation Interferometers: Applications in Microscopy and Macroscopy* (New York: Wiley-Interscience) p. 21

[22] Zhang C M, Xiang L B, Zhao B C and Yuan X J 2002 *Opt. Commun.* **203** 21

[23] Zhang C M, Zhao B C and Xiang L B 2004 *Appl. Opt.* **43** 6090

[24] Wu L, Zhang C M and Zhao B C 2007 *Opt. Commun.* **273** 67

[25] Wu J F, Zhang C M, Zhang Y T, Liu H C and Zhai X J 2008 *Chin. Phys.* B **17** 2504

[26] Zhang C M, Xiang L B and Zhao B C 2000 *SPIE* **4087** 957

[27] Zhang C M, Zhao B C and Xiang L B 2003 *Opt. Commun.* **227** 221

[28] Zhang C M, Xiang L B and Zhao B C 2004 *J. Opt.* A: *Pure Appl. Opt.* **6** 815

[29] Zhang C M, Zhao B C, Yuan Y and He J 2006 *SPIE* **6032** 60320T1
[30] Zhang C M, Xiang L B, Zhao B C, Li Y C and Peng Z H 2006 *SPIE* **6150** 615001
[31] Zhang C M, Zhao B C, Yuan Z L and Huang W J 2009 *J. Opt.* A: *Pure Appl. Opt.* **11** 085401
[32] Mu T K, Zhang C M and Zhao B C 2009 *Opt. Commun.* **282** 1984
[33] Mu T K, Zhang C M and Zhao B C 2009 *Appl. Opt.* **48** 2333
[34] Mu T K, Zhang C M and Zhao B C 2009 *Acta Phys. Sin.* **58** 3877 (in Chinese)
[35] Peng Z H, Zhang C M, Zhao B C, Li Y C and Wu F Q 2006 *Acta Phys. Sin.* **55** 6374 (in Chinese)
[36] Yuan Z L, Zhang C M and Zhao B C 2007 *Acta Phys. Sin.* **56** 6413 (in Chinese)
[37] Du J, Zhang C M, Zhao B C and Sun Y 2008 *Acta Phys. Sin.* **57** 6311 (in Chinese)
[38] Jian X H, Zhang C M, Zhu B H, Zhao B C and Du J 2008 *Acta Phys. Sin.* **57** 7565 (in Chinese)
[39] Jian X H, Zhang C M, Zhao B C, Zhang L and Zhu L Y 2009 *Acta Phys. Sin.* **58** 2286 (in Chinese)
[40] Ren W Y, Zhang C M and Mu T K 2009 *Chin. Phys. Lett.* **26** 084209
[41] Zhang C M, Ren W Y and Mu T K 2010 *Chin. Phys.* B **19** 024202
[42] Wu J F and Zhang C M 2010 *Chin. Phys.* B **19** 034201
[43] Junttila M L, Kauppinen J and Ikonen E 1991 *J. Opt. Soc. Am.* A **8** 1457
[44] Chamberlin J 1979 *The Principles of Interferometric Spectroscopy* (Chichester: Wiley Interscience) p. 95
[45] Rafert J B, Sellar R G and Blatt J H 1995 *Appl. Opt.* **34** 7228
[46] Tropf W J, Thomas M E and Harris T J 1995 *Properties of Crystals and Glasses* Chapter 33 in Vol. 2 *Handbook of Optics* (New York: McGraw-Hill) pp. 33, 62